# Electronic Structure of Regular Bacterial Surface Layers

Denis V. Vyalikh,[1] Steffen Danzenbächer,[1] Michael Mertig,[2] Alexander Kirchner,[2] Wolfgang Pompe,[2] Yuriy S. Dedkov,[1] and Serguei L. Molodtsov[1,*]

[1]*Institut für Festkörperphysik, Technische Universität Dresden, D-01062 Dresden, Germany*

[2]*Max-Bergmann-Zentrum für Biomaterialien and Institut für Werkstoffwissenschaft, Technische Universität Dresden, D-01062 Dresden, Germany*

(Received 16 June 2004; published 1 December 2004)

We report photoemission and near-edge x-ray absorption fine structure measurements of the occupied and unoccupied valence electronic states of the regular surface layer of *Bacillus sphaericus,* which is widely used as the protein template for the fabrication of metallic nanostructures. The two-dimensional protein crystal shows a semiconductorlike behavior with a gap value of ~3.0 eV and the Fermi energy close to the bottom of the lowest unoccupied molecular orbital. We anticipate that these results will open up new possibilities for the electric addressability of biotemplated low-dimensional hybrid structures.

DOI: 10.1103/PhysRevLett.93.238103 PACS numbers: 87.68.+z, 73.22.–f, 87.14.Ee, 87.64.Gb

Controlled organization of matter at the molecular scale is an important objective of materials science, aiming at the development of reliable bottom-up strategies for the miniaturization of electronic components. Addressing fundamental issues of both nanometer fabrication and supramolecular engineering, biomolecular templating has demonstrated the capability of building up thoroughly predefined inorganic nanostructures by taking advantage of the unique self-assembly capabilities of biomolecules and of their well-defined structural and physicochemical properties [1]. In particular, the precise control of the association of metallic nanoparticles to DNA and proteins [2] and the direct nucleation and growth of metal clusters on biomolecular templates [3–5] have led to metallo-organic nanostructures with structural densities much higher than those of today's microelectronic structures [6]. It is expected that these novel hybrid materials can disclose new, still not discovered fascinating phenomena. In analogy with a series of organic and molecular systems [7,8], the synthesized composites might reveal, e.g., superconducting or low-dimensional magnetic behavior because of both the onset of size-dependent quantum effects and the increase of the surface-to-volume ratio with decreasing particle size.

However, both the understanding and the tailoring of the physical and chemical properties of biotemplated hybrid systems do not only require knowledge about the electronic properties of the metallic clusters but also thorough information about the electronic structure of the template. With a few exceptions, these data are lacking. Theoretical investigations are difficult to perform because of the large size of unit cells [9–11]. Spectroscopic methods like photoemission (PE) and near-edge x-ray absorption fine structure (NEXAFS) spectroscopy provide the most direct information about electronic structure. However, so far NEXAFS is rarely [12,13] and PE is not applied to biological substances because intensive photon exposure easily destroys the specimen. Another methodical obstacle is that particularly PE experiments require samples with atomically clean surfaces that might be difficult to assure by *ex situ* sample preparation. Moreover, the interpretation of the spectroscopic data might fail, if the biological units consist of a large amount of atoms. Thus, so far only a few rather indirect measurements of the electronic structure are performed by nuclear magnetic resonance [14], electron paramagnetic resonance [15], fluorescence-excitation spectroscopy [16], or electronic circular dichroism [17].

Here we report PE and partial-electron-yield NEXAFS measurements of the electronic structure of regular bacterial surface layers (S layer), which comprise the first PE studies on valence electronic states in proteins. S layers are regular two-dimensional (2D) protein crystals, which form the outermost cell envelope component of many prokaryotes in almost all phylogenetic branches of bacteria and archaea [18]. The precise spatial modulation of the physicochemical surface properties of the periodic protein crystal makes them an ideal matrix for supramolecular engineering. We investigate the electronic structure of the S layer of *Bacillus sphaericus NCTC 9602,* which is frequently used as a 2D template for the fabrication of highly oriented metallic nanocluster arrays [4,5]. The 5.0 nm thick protein layer exhibits a p4 symmetry, a lattice constant of 12.5 nm, and a complex pattern of pores and gaps that are 2 nm wide (Fig. 1). The S-layer subunits have a molecular weight of 111.5 kDa. As the main result, we found a semiconductorlike electronic structure with the Fermi level located at the bottom of the lowest unoccupied molecular orbital (LUMO). This investigation gives new insight into the understanding of the electronic structure of complicated protein structures and their application in bionanotechnology.

Regular S-layer sheets, isolated from the cell walls of *B. sphaericus NCTC 9602* [5], were deposited *ex situ* onto plasma-treated naturally oxidized Si substrates ($SiO_x$/Si) before injecting them into the ultrahigh vacuum spectrometer chamber. Resembling spectroscopic

 

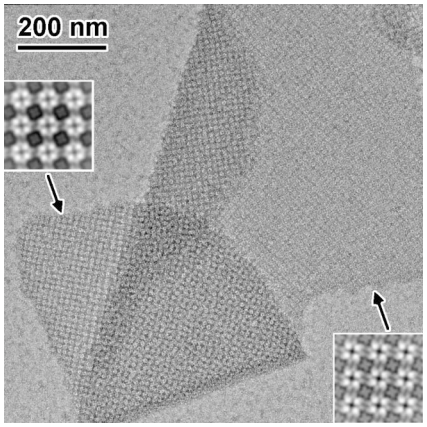


FIG. 1. Transmission electron micrograph of a folded, negatively stained sheet of the S layer of *B. sphaericus NCTC 9602*. Both insets have a size of $38 \times 38$ nm$^2$, and depict image-reconstructed parts of the S-layer sheet with different orientations to the surface demonstrating the morphological anisotropy of the "inner" and the "outer" surface of the S layer.

results were obtained for a large number of sample preparations, giving strong evidence of only negligible (if any) surface contaminations. The experiments were performed at BESSY (Berlin) using radiation from the Russian-German ultrahigh energy-resolution dipole beam line. In contrast to nowadays mostly employed undulator beam lines, which deliver an extremely high photon flux in the form of a discrete spectrum, this beam line provides low-intensity radiation continuously distributed in a wide range of photon energies (30 to 1500 eV) and is thus suitable for spectroscopic studies of "fragile" protein samples. C 1*s* NEXAFS spectra of the S layer were taken with a photon-energy resolution of 80 meV full width at half maximum (FWHM). The spectra were normalized to the signal measured for a clean Si wafer. In the PE measurements, a photon energy of 40.8 eV (He II$\alpha$) was selected to compromise between the high photoexcitation cross sections of the primarily $2p$ states of the second-period elements forming the valence bands of proteins, and the high surface sensitivity, required to increase the contribution from the valence band of the S layer relatively to the signal from the substrate. The overall PE energy resolution was set to 150 meV FWHM. In both experiments, the photon incident angle was selected to be 50° relative to the sample surface [19]. The light-spot size at the sample position was $20 \times 80$ $\mu$m$^2$ providing the possibility to study the homogeneous parts of the S layers. Only a moderate S-layer dynamic charging at a level similar to that of regular wide-gap semiconductors was observed with PE. This fact reveals relatively large charge carrier mobility suggesting a bandlike description of the electronic structure of the S layer.

NEXAFS spectroscopy probes the energy- and angular-momentum character dependent photoabsorption cross sections of core-electron excitations into such unoccupied electronic states, which are primarily localized on the excited atoms [20]. As each atom has characteristic binding energies (BE) of core levels, NEXAFS spectra reflect the element-specific density of empty states in compounds. Since S layers contain mainly C atoms involved in different forms of bonding, the most informative spectra to be studied are those taken upon excitation of the C 1*s* core level [21]. The C 1*s* spectrum reflecting the partial density of the C $2p$ unoccupied electronic states of the "as-deposited" S layer (Fig. 2 top) is found to be surprisingly simple. It shows rather sharp transitions involving $\pi^*$-symmetry molecular orbitals (283–289 eV) and smooth structures in the $\sigma^*$-transition region (>290 eV). The observed spectral features disappear almost completely when the sample is disintegrated applying high-flux irradiation with non-monochromatized, zero-order light (inset in Fig. 2).

The $\sigma^*$-transition structures observed for the as-deposited S layer are very broad because of the short lifetime of the corresponding exciting states. Here we concentrate on the evaluation of the $1s \rightarrow \pi^*$ resonances. These are found to be similar to those measured for individual amino acids and small peptides [12]. We interpret the $\pi^*$-transition spectrum of the S layer within a simple "building-block model" where the complex protein structure is seen as an assembly of its primary constituents. In comparison to data obtained for a set of different amino acids [12] and their interpretation on the basis of the *ab initio* static-exchange method calculations [22], we can assign the lowest energy $\pi^*$ feature of the S-layer spectrum at 285.0 eV to transitions mainly into unoccupied orbitals of C═C double bonds located in the aromatic rings of individual amino acids. The LUMO-derived lowest energy feature is manifold since the en-

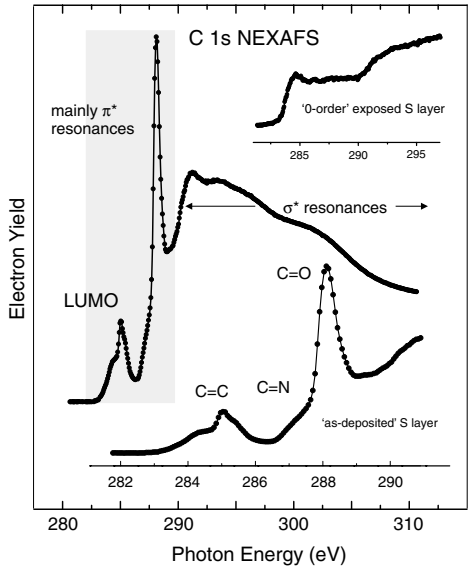


FIG. 2. C 1*s* NEXAFS spectra of the S layer taken before and after (upper inset) its exposure with the "zero-order" synchrotron radiation. The region of the $\pi^*$ resonances (shadowed) is enlarged in the bottom.

ergies of the particular C═C orbitals depend on the specific molecular environment of the C atoms which participate in the double bonds. The second peak at 288.1 eV photon energy is of much larger intensity and can predominantly be attributed to the $1s \rightarrow \pi^*$ excitation of the C═O double bonds of the carboxyl groups. There is no initial-state splitting of this resonance since the chemical environment of this bond does not change from one amino acid to another. Correspondingly, this feature appears less structured than the 285-eV one. The shoulder at the low-energy side of the C═O peak at ~287 eV coincides in energy with the expected C═N $1s \rightarrow \pi^*$ resonance, which is not supposed to reveal a pronounced manifold splitting by the same reason as discussed for the C═O transition. By referring the N 1*s* and O 1*s* NEXAFS spectra of the S layer (not shown) to the same energy scale according to the BEs of the corresponding core levels, the $\pi^*$-derived peaks of the N 1*s* and O 1*s* spectra overlap with the 287-eV and 288.1-eV features of the C 1*s* spectrum, supporting the interpretation of these two structures in terms of C═N and C═O bonds, respectively. Since the intensity ratios between the three main features of the $\pi^*$-transition region in the C 1*s* spectrum are mainly caused by the relative numbers of bonds contributing to a particular bond type (C═C, C═O, or C═N), we can conclude that the relative number of amino acids with aromatic rings in the studied S layer is rather small. This is in agreement with the investigation of the primary protein structure, reporting for the S layer of *B. sphaericus NCTC 9602* a content of amino acids with aromatic rings of less than 11% [23].

The occupied electronic states were studied by angle-integrated valence-band PE. The corresponding spectrum [Fig. 3(a)] contains contributions from the S layer and the substrate. In order to extract the virginal signal of the S layer, the bare plasma-treated substrate was measured before at the same photon energy (shadowed area in Fig. 3). The substrate spectrum reveals a triplet line shape, which is a combination of a typical $SiO_x$ valence-band spectrum with a pronounced O 2*p* derived feature and structures characteristic for admixtures of different Si carbides [24]. The pure S-layer spectrum [Fig. 3(b)] was obtained by a subtraction of the shadowed spectrum from the top one [25]. Similar to results obtained for other organic materials, the S-layer PE spectrum consists of a series of individual peaks that originate from different molecular orbitals. The highest occupied molecular orbital (HOMO) of the S layer is relatively sharp. A second, intense manifold structure (*A*) is located ~4.5 eV below the HOMO, and a less pronounced peak (*B*) is found at 21 eV.

Valence-band PE is not element specific. Hence, from PE data we cannot unambiguously determine the origin of the occupied molecular orbitals, particularly, since electronic structure calculations do not exist for S layers. However, preliminary interpretation can be derived from electronic density-of-states (DOS) calculations for rather small proteins [9–11], assuming that integral DOS data can be expected to be qualitatively similar for different proteins. Theoretical evidence for this assumption is reported for the comparison of the DOS for peptidic Bunodosoma granulifera toxin and charybdotoxin [9,10] as well as for self-assembled peptide nanotubes [11] calculated using the local density approximation. In Fig. 4 the electronic structure of the S layer is compared with the calculated DOS of peptidic charybdotoxin. To construct the experimental electronic structure of the S layer, the occupied and unoccupied electronic states, probed by PE and NEXAFS, are referred to the common Fermi energy ($E_F$). The $E_F$ position of the PE spectrum was determined by measuring the $E_F$ offset for a reference metallic gold sample. In addition, the BE shifts of the S-layer PE features induced by charging of the bare protein sample were accounted for by a separate PE experiment with S layers covered with a thin gold film. The latter system was found to be metallic, and the gold does not noticeably react with the protein template, since the PE line shapes are very similar to those of the pristine S-layer sample. The NEXAFS data were referred to $E_F$ by using the BE of the S-layer C 1*s* PE spectrum assuming a similar screening of the remaining core holes in x-ray absorption and photoemission processes. Although the effect of the core hole was found to be rather strong in 1D ladderlike structures (e.g., naphthacene, $C_{18}H_{12}$), its magnitude decreases with the increase of the size and dimensionality of the $\pi$-conjugated system [26]. By the observed similarity of energies and line shapes of the calculated and the measured structures in Fig. 4, we can assign the occupied valence-band PE features on the basis of the eigenvector analysis performed in [9]. According to this, the main contributions to the HOMO origi-

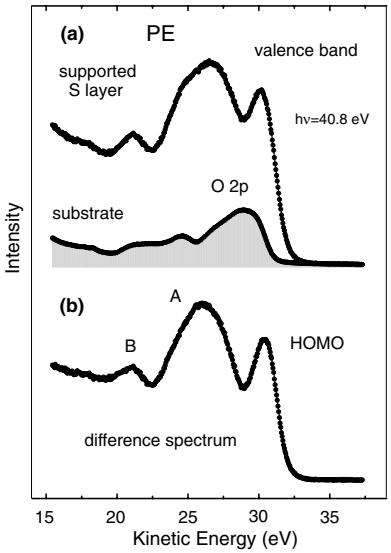


FIG. 3. (a) Valence-band PE spectra of the supported S layer and of the pure substrate (shadowed). (b) Difference spectrum, which represents the pure PE signal from the S layer.

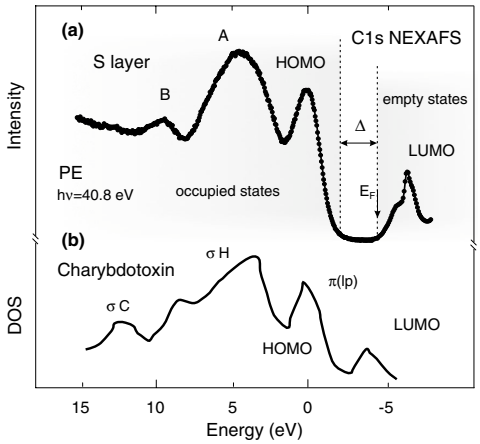


FIG. 4. (a) Valence-band and LUMO originating structure of the S layer as derived from the PE and NEXAFS experiments. (b) DOS calculated for charybdotoxin [9]. The energy scales are adjusted relatively to the positions of the HOMOs.

nate from $\pi$ clouds of aromatic rings and from lone pairs of oxygen and nitrogen. Feature *A* is mainly caused by the $\sigma$-bondlike structures between hydrogen and carbon atoms, whereas feature *B* arises from the $\sigma$ bonds between C atoms. The calculated energy gap between LUMO and HOMO is somewhat smaller than the measured one, which is a known effect for calculations of semiconductor band structures within density functional theory [27].

The electronic structure of the 2D protein layer shown in Fig. 4 resembles that of a moderate wide-gap semiconductor. The energy gap value is $\Delta \sim 3.0$ eV. As an important feature, we find the Fermi level closely located to the bottom of the LUMO. The gained information is of high importance to make reliable predictions for possible chemical reactions and other chemical or physical phenomena in hybrid biological systems. In particular, we expect that—similarly to the behavior of $C_{60}$ films—the Fermi level of the investigated protein can be shifted to higher energies by intercalation of dopants. Since the LUMO is formed by the C-derived states, and C atoms exhibit a large electronegativity, we anticipate that intercalation of the S layer with donors might lead to a filling of the LUMO. Similarly to other molecular compounds like alkali fullerides [8] it may even cause high-temperature superconductivity of the S-layer intercalation compounds, which could be used, e.g., in field-effect transistor doped biocomposites. This will, in general, open the possibility to use the S layers to address clusters arrays, grown on the template, electronically. It seems also conceivable to obtain a local addressability of individual or a limited number of clusters by a patterned intercalation of dopants, e.g., by vapor deposition of donor materials through a lithographic mask.

This work was supported by the DFG (Grants No. PO392/18 and No. SFB463), by the BMBF (Grant No. 13N8145), by the SMWK, and by the EU (FP5, Contract No. G5RD-CT-2002-0750). We acknowledge the help of Reiner Wahl with TEM.

*Electronic address: molodtso@physik.phy.tu-dresden.de

[1] S. Mann, Nature (London) **365**, 499 (1993).
[2] R. Elghanian *et al.*, Science **277**, 1078 (1997); A. P. Alivisatos *et al.*, Nature (London) **382**, 609 (1996); S. R. Hall *et al.*, Chem. Phys. Chem. **3**, 184 (2001).
[3] E. Braun *et al.*, Nature (London) **391**, 775 (1998); M. Mertig *et al.*, Nano Lett. **2**, 841 (2002); W. Shenton *et al.*, Nature (London) **389**, 585 (1997).
[4] S. Dieluweit *et al.*, Supramolecular Sci. **5**, 15 (1998); M. Mertig *et al.*, Eur. Phys. J. D **16**, 317 (2001).
[5] R. Wahl *et al.*, Adv. Mater. **13**, 736 (2001).
[6] M. Mertig *et al.*, Eur. Phys. J. D **9**, 45 (1999).
[7] *Organic Superconductivity*, edited by V. Z. Kresin and W. A. Little (Plenum Press, New York, 1990); S. Uji *et al.*, Nature (London) **410**, 908 (2001); A. Schindler *et al.*, Europhys. Lett. **58**, 885 (2002); E. Huger and K. Osuch, Europhys. Lett. **63**, 90 (2003).
[8] A. F. Hebard *et al.*, Nature (London) **350**, 600 (1991); S. P. Kelty *et al.*, Nature (London) **352**, 223 (1991).
[9] J. Ireta *et al.*, J. Am. Chem. Soc. **120**, 9771 (1998).
[10] F. Aparicio *et al.*, J. Phys. Chem. B **107**, 1692 (2003).
[11] P. Carloni *et al.*, Phys. Rev. Lett. **79**, 761 (1997).
[12] J. Boese *et al.*, J. Electron Spectrosc. Relat. Phenom. **85**, 9 (1997); K. Kaznacheyev *et al.*, J. Phys. Chem. A **106**, 3153 (2002).
[13] A. P. Hitchcock *et al.*, J. Biomater. Sci., Polymer Ed. **13**, 919 (2002).
[14] Alia *et al.*, J. Am. Chem. Soc. **123**, 4803 (2001).
[15] Alia *et al.*, Chem. Phys. **294**, 459 (2003).
[16] A. M. van Oijen *et al.*, Science **285**, 400 (1999).
[17] J. D. Hirst *et al.*, J. Phys. Chem. B **107**, 11813 (2003).
[18] U. B. Sleytr *et al.*, *Crystalline Bacterial Cell Surface Proteins* (Academic Press, San Diego, 1996).
[19] The line shapes of C 1*s*, N 1*s*, and O 1*s* NEXAFS spectra are independent on the light polarization pointing to the nonoriented origin of the chemical bonds in the S layer.
[20] H. Ade and S. G. Urquhart, in *Chemical Applications of Synchrotron Radiation*, edited by T. K. Sham (World Scientific, Singapore, 2002).
[21] The upper contribution limit of the residual C contaminations from the substrate was measured from freshly plasma-treated Si wafers and estimated to be negligible as compared to the signal acquired from the S layer.
[22] V. Carravetta *et al.*, J. Chem. Phys. **109**, 1456 (1998).
[23] Nucleotide Sequence Database of the European Molecular Biology Laboratory (http://www.ebi.ac.uk).
[24] R.-C. Fang and L. Ley, Phys. Rev. B **40**, 3818 (1989).
[25] To this aim, the two spectra were normalized to the photon flux, and the substrate spectrum was additionally scaled accounting for both calculated attenuation of photoelectrons in the S layer [M. P. Seah and W. A. Dench, Surf. Interface Anal. **1**, 2 (1979)] and the degree of the S-layer coverage estimated from scanning electron microscopy data (not shown).
[26] H. Oji *et al.*, J. Chem. Phys. **109**, 10409 (1998).
[27] H. Eschrig *et al.*, Solid State Commun. **56**, 773 (1985).